The Astrophysical Journal Letters, 907:L19 (12pp), 2021 January 20 https://doi.org/10.3847/2041-8213/abd5b7


# Massive Stellar Triples Leading to Sequential Binary Black Hole Mergers in the Field

Alejandro Vigna-Gómez[1], Silvia Toonen[2], Enrico Ramirez-Ruiz[1,3], Nathan W. C. Leigh[4,5], Jeff Riley[6,7], and Carl-Johan Haster[8,9]

[1] DARK, Niels Bohr Institute, University of Copenhagen, Jagtvej 128, DK-2200, Copenhagen, Denmark; avignagomez@nbi.ku.dk
[2] Institute of Gravitational Wave Astronomy, School of Physics and Astronomy, University of Birmingham, Birmingham, B15 2TT, UK
[3] Department of Astronomy and Astrophysics, University of California, Santa Cruz, CA 95064, USA
[4] Departamento de Astronomía, Facultad de Ciencias Físicas y Matemáticas, Universidad de Concepción, Concepción, Chile
[5] Department of Astrophysics, American Museum of Natural History, New York, NY 10024, USA
[6] Monash Centre for Astrophysics, School of Physics and Astronomy, Monash University, Clayton, VIC 3800, Australia
[7] The ARC Centre of Excellence for Gravitational Wave Discovery—OzGrav, Australia
[8] LIGO Laboratory, Massachusetts Institute of Technology, 185 Albany St., Cambridge, MA 02139, USA
[9] Department of Physics and Kavli Institute for Astrophysics and Space Research, Massachusetts Institute of Technology, 77 Massachusetts Ave., Cambridge, MA 02139, USA

*Received 2020 October 26; revised 2020 December 16; accepted 2020 December 21; published 2021 January 21*

## Abstract

Stellar triples with massive stellar components are common and can lead to sequential binary black hole mergers. Here we outline the evolution toward these sequential mergers and explore these events in the context of gravitational-wave astronomy and the pair-instability mass gap. We find that binary black hole mergers in the pair-instability mass gap can be of triple origin and therefore are not exclusively formed in dense dynamical environments. We discuss the sequential merger scenario in the context of the most massive gravitational-wave sources detected to date: GW170729 and GW190521. We propose that the progenitor of GW170729 is a low-metallicity field triple. We support the premise that GW190521 could not have been formed in the field. We conclude that triple stellar evolution is fundamental to the understanding of gravitational-wave sources and likely other energetic transients as well.

*Unified Astronomy Thesaurus concepts:* Astrophysical black holes (98)

## 1. Introduction

The importance of interactions between massive stars in isolated binaries has become increasingly recognized in recent decades (e.g., Podsiadlowski et al. 1992; Sana et al. 2012). Recent studies indicate that early B-type and O-type stars are almost exclusively part of higher-order configurations, such as triple and quadruple systems (Sana et al. 2014; Moe & Di Stefano 2017). If future surveys confirm this, our understanding of massive stellar evolution will have to include the increased complexity of multiple-body interactions that were previously mostly considered in dense dynamical environments such as nuclear, globular, or open clusters (e.g., Sigurdsson & Hernquist 1993; Leigh & Geller 2013).

An alternative to electromagnetic methods to study high-mass stellar multiplicity is gravitational-wave (GW) astronomy, as massive stars are believed to be the progenitors of stellar-mass black holes (BHs). Stellar-mass binary black holes (BBHs) are believed to form predominantly in field binaries (e.g., Belczynski et al. 2002; Neijssel et al. 2019) and clusters (e.g., Portegies Zwart & McMillan 2000; Leigh et al. 2014; Rodriguez et al. 2019). There have been efforts to try to understand how best to segregate these two different origins, mostly based on eccentricities and spins, yet there is no definitive consensus on the origin of current GW sources (e.g., Abbott et al. 2019).

One candidate signature for the cluster origin of a GW is a BH mass in the pair-instability supernova (PISN) mass gap.[11] The PISNe are initiated by an electron–positron pair instability that eventually leads to explosive oxygen burning in the core of massive stars (see Langer 2012, and references therein). The PISNe do not leave behind remnants; therefore, a gap is expected in the mass distribution of BHs for stars with helium core masses in the range of ≈64–133 $M_{\odot}$ (Heger & Woosley 2002). Consequently, isolated binary evolution theory does not predict individual BHs in that regime (Stevenson et al. 2019; van Son et al. 2020). As multiple BH mergers can populate the mass gap, the discovery of BBH systems with one component lying within the mass gap has been considered a smoking gun for cluster origin (Rodriguez et al. 2019; Samsing & Hotokezaka 2020). The recent detection of GW190521 (Abbott et al. 2020a), with at least one BH within the mass gap, adds to the conundrum.

Here we give an overview of which isolated massive stellar triples experience a *sequential merger* of BBHs. We investigate the potential origin of such configurations, put them in the context of GW observations, and focus on the masses and spins of sequential mergers leading to BBHs in the mass gap. We propose that GW170729 is of isolated triple origin and suggest that the mass gap event GW190521 was not formed in the field. Finally, we highlight the importance of massive stellar triples in a broader astronomical context.

## 2. Method

Here we outline our main assumptions for the key physics of the formation of a sequential merger starting at the zero-age main sequence. We consider isolated hierarchical triple systems, composed of an inner binary with masses $M_1 \geqslant M_2$ and an outer companion of mass $M_3$. In the sequential mergers that we consider here, the inner BBH merges first, and afterward, the

[11] https://compas.science/

[10] In this Letter, we do not consider the potential mass gap between massive neutron stars and low-mass BHs.

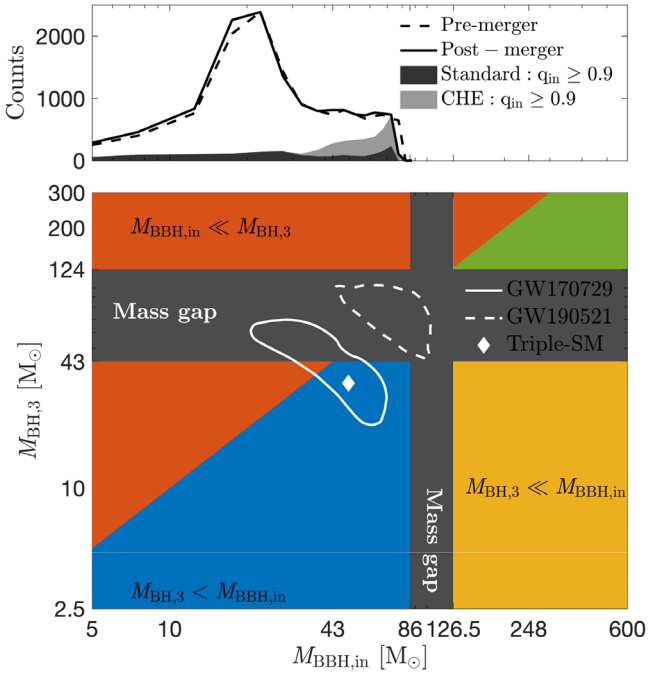


**Figure 1.** Overview of mass combinations for isolated triples leading to sequential mergers. Top panel: mass distribution of merging BBHs for the inner binary based on isolated binary evolution calculations (Riley et al. 2020). The solid (dashed) black line is the mass distribution after (before) the inner BBH merger. Shaded regions highlight standard evolving (dark gray) and CHE (light gray) systems with $q_{in} \geqslant 0.9$. Bottom panel: the gray area is the approximate mass gap region where BHs of isolated binary origin are not expected to form due to PISNe (Section 3.1). The colored regions are described in Section 3.1, and examples are illustrated in Figure 3. The diamond is an example of a sequential merger (Triple-SM), as discussed in Section 3.4. White solid and dashed contours are the 90% confidence intervals for GW170729 (Chatziioannou et al. 2019) and GW190521 (Abbott et al. 2020a), respectively.

remnant merges with the outer BH. We adopt circular coplanar prograde orbits, as supported by observations of compact triples (Tokovinin 2017). For circular coplanar prograde orbits, we do not expect Lidov–Kozai cycles and neglect other three-body dynamical effects (see, e.g., Naoz 2016, for a review).

The triple must remain dynamically stable from the zero-age main sequence until the inner BBH merger, which holds if (Mardling & Aarseth 2001)

$$\frac{a_{\rm out}}{a_{\rm in}} \geqslant \left(\frac{a_{\rm out}}{a_{\rm in}}\right)_{\rm crit} \equiv \frac{2.8}{1-e_{\rm out}}\left[\frac{(1+q_{\rm out})(1+e_{\rm out})}{\sqrt{1-e_{\rm out}}}\right]^{2/5}, \quad (1)$$

where $a$ is the semimajor axis, $e$ is the eccentricity, and $q$ is the mass ratio (the inner and outer orbits are specified by the *in* and *out* subscripts). The outer mass ratio is $q_{\rm out} \equiv M_3/(M_1+M_2)$.

We use the synthetic BBH population from Riley et al. (2020) based on isolated binary evolution to investigate the orbital properties of the inner binary (see Appendix A for further details). The models include mass loss, mass transfer, supernovae, and chemically homogeneous evolution (CHE). In Figure 1, we present the intrinsic mass distribution of merging BBHs. We focus on low-metallicity stars ($Z \lesssim 10^{-3}$) in order to neglect mass loss, spin-down, and orbital changes due to stellar winds.

As each star of the triple evolves, it will eventually become a BH with mass $M_{{\rm BH},i}$ (with $i = 1, 2, 3$), for which we assume the following. The BHs have a minimum mass of $M_{\rm BH,min} = 2.5\,M_\odot$. There is a mass gap in the range $43 \lesssim M_{\rm gap}/M_\odot \lesssim 124$ (du Buisson et al. 2020) due to PISNe. The exact lower limit of the mass gap is uncertain and might be as high as $M_{\rm BH} \approx 50\,M_\odot$ (for an overview, see Stevenson et al. 2019, and references therein). Furthermore, we assume that stars with carbon–oxygen core masses above $11\,M_\odot$ experience complete fallback (Fryer et al. 2012) and negligible neutrino mass loss (Müller et al. 2016), likely suppressing BH natal kicks. All BHs are born as slow rotators (Fuller & Ma 2019).

During the inner BBH merger, mass is lost by radiation from the center of mass of the merging BBH. This leads to a GW Blaauw kick similar to that in spherically symmetric supernovae (Blaauw 1961). The fraction of radiated mass with respect to the mass of the merging BBH ($f_{\rm rad}$) depends on the masses and spins of the system (Appendix B). This modifies the orbit of the tertiary,

$$\frac{a_{\rm out,post}}{a_{\rm out,pre}} = \left[2 - \frac{M_{\rm BH,1}+M_{\rm BH,2}+M_{\rm BH,3}}{M_{\rm BBH,in}+M_{\rm BH,3}}\right]^{-1}, \quad (2)$$

and

$$e_{\rm out,post} = \frac{f_{\rm rad}\,(M_{\rm BH,1}+M_{\rm BH,2})}{M_{\rm BBH,in}+M_{\rm BH,3}}, \quad (3)$$

where $M_{\rm BBH,in} \approx (1-f_{\rm rad})(M_{\rm BH,1}+M_{\rm BH,2})$. For nonspinning BBHs and assuming $e_{\rm out,pre} \approx 0$, $f_{\rm rad} \approx 0.05$, $e_{\rm out,post} \approx 0.05$, and $a_{\rm out,post} \approx 1.06 \times a_{\rm out,pre}$. Furthermore, conservation of momentum gives rise to a recoil kick, which has a magnitude of zero when $q_{\rm BBH,in} \approx 0$ or 1 and can be as high as $v_{\rm recoil} \lesssim 175\,{\rm km\,s^{-1}}$ for $q_{\rm BBH,in} \approx 0.36$ (González et al. 2007). As our synthetic population favors $q_{\rm BBH,in} \gtrsim 0.9$ (Figures 1 and 2), the magnitude of the recoil kick should be small, and we ignore it. The radiated mass fraction is maximal ($f_{\rm rad,max} \approx 0.12$) when we consider a merger from an equal-mass maximally spinning BBH that is aligned with the orbital spin. This constrains the postmerger eccentricity and separation to $e_{\rm out} \lesssim 0.14$ and $a_{\rm out,post} \lesssim 1.16 \times a_{\rm out,pre}$, respectively. Therefore, the systems we consider here cannot be unbound during the inner BBH merger.

We assume the outer orbit is almost circular at all times. In this case, the GW inspiral time can be approximated with (Peters 1964)

$$T_c \approx \frac{5}{256}\frac{c^5 a_{\rm out}^4}{G^3 M_{\rm BBH,in} M_{\rm BH,3}(M_{\rm BBH,in}+M_{\rm BH,3})}. \quad (4)$$

We estimate the effective spin of the sequential merger as

$$\chi_{\rm eff} = \frac{(M_{\rm BBH,in}\boldsymbol{\chi}_{\rm BBH,in} + M_{\rm BH,3}\boldsymbol{\chi}_{\rm BH,3})\cdot \hat{L}_{\rm N}}{M_{\rm BBH,in}+M_{\rm BH,3}} = \frac{|\boldsymbol{\chi}_{\rm BBH,in}|}{1+M_{\rm BH,3}/M_{\rm BBH,in}}, \quad (5)$$

where $\boldsymbol{\chi}$ is the dimensionless component spin of the BH and $\hat{L}_{\rm N}$ is the unit vector parallel to the system's orbital angular momentum. For a merger of an equal-mass inner nonrotating BBH, the remnant has a spin magnitude of $|\boldsymbol{\chi}_{\rm BBH,in}| \approx 0.68$ (Boyle et al. 2008).

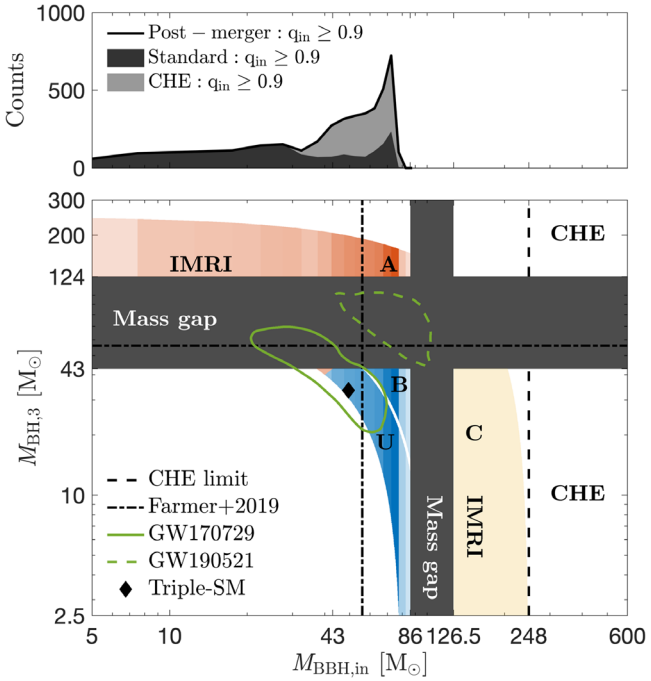


**Figure 2.** Overview of mass combinations for isolated triples leading to sequential mergers with total mass in the (PISN) mass gap. Similar to Figure 1 but only accounting for sequential mergers that have a final total mass within the mass gap. For the mass of the inner BBH, the intensity of the color reflects the bin weight from the mass histogram (top panel). We explore mass gap sequential mergers in the red (A), blue (B), and yellow (C) regions (see Section 3.3 for full description). Blue region B only includes sources well within the mass gap with total mass $(M_{BBH,in} + M_{BH,3})/M_\odot > 100$. To incorporate model uncertainties, we lower the threshold to the range $80 \leqslant (M_{BBH,in} + M_{BH,3})/M_\odot \leqslant 100$ (Stevenson et al. 2019) for region U. The black dashed–dotted line at $M_{BBH,in} = 56\,M_\odot$ corresponds to the maximum single BH mass according to Farmer et al. (2019). The area to the right of this limit and left of the mass gap is not populated by single stellar evolution. The black dashed line corresponds to $2 \times M_{gap,max} \approx 248\,M_\odot$, the minimum combined mass for CHE BBHs above the mass gap (du Buisson et al. 2020). The intermediate mass-ratio inspirals (IMRIs) can be in the red and yellow regions. See Figure 1 for further explanation and Figure 3 for an illustration of the evolution of these systems.

## 3. Results

### 3.1. BH Mass Parameter Space for Sequential Mergers

In Figure 1, we display the possible mass combinations of inner BBHs and outer BHs for sequential mergers. We denote the (PISN) mass gap in gray. Assuming single stellar evolution for the tertiary, the mass gap for the outer BH is in the range $M_{gap,min} = 43\,M_\odot \lesssim M_{BH,3} \lesssim M_{gap,max} = 124\,M_\odot$. The corresponding mass gap for the inner BBH is shifted to $2 \times M_{gap,min} = 86\,M_\odot \lesssim M_{BBH,in} \lesssim M_{gap,max} + M_{BH,min} = 126.5\,M_\odot$.

In Figure 1, we classify four regions of interest: red, blue, yellow, and green. The red region comprises $M_{BBH,in} < M_{BH,3}$, where the outer (more massive) BH collapses before the other BHs form, based on stellar evolution timescales. The blue region comprises $M_{BH,3} < M_{BBH,in}$, with $M_{BBH,in} \lesssim 86$ and $M_{BH,3} \lesssim 43\,M_\odot$. Most GW sources detected to date are in the red and blue regions below the mass gap (Abbott et al. 2019). The yellow region comprises $M_{BBH,in} \gtrsim 126.5\,M_\odot$, with $M_{BBH,in} \gg M_{BH,3}$ and $M_{BH,3} \lesssim M_{gap,min} \approx 43\,M_\odot$. Finally, the green region comprises $M_{BBH,in} > M_{BH,3}$, with $M_{BBH,in} \gtrsim 126.5$ and $M_{BH,3} \gtrsim 124\,M_\odot$. The rare sequential mergers from the green region will have masses above the mass gap and are not discussed any further.

### 3.2. Types of Triples

For the evolution of the stars, we consider standard evolving and compact constituent stars. Standard evolving stars rotate slowly, develop a composition gradient, and can expand up to thousands of solar radii during their evolution (e.g., Podsiadlowski et al. 1992). This expansion is avoided by stars in metal-free (Population III) environments (Marigo et al. 2001), in certain mass–metallicity regimes (Shenar et al. 2020), or that rotate rapidly such that rotational mixing is induced (Maeder 1987), i.e., CHE. The orbits of CHE binaries can therefore remain more compact throughout their evolution to BBH formation as compared to binaries with standard evolving stars (de Mink & Mandel 2016; Marchant et al. 2016; Riley et al. 2020). This is favorable for the sequential merger channel in order for the triple to remain dynamically stable and compact enough to lead to two mergers within a Hubble time (Equations (1) and (4)). We therefore consider four distinct types of stellar triples (illustrated in Figure 3): (1) an inner binary with compact stars and an outer standard evolving star, (2) all compact stars, (3) at least one standard evolving star in the inner binary with an outer standard evolving companion, and (4) at least one standard evolving star in the inner binary with an outer compact star.

### 3.3. Populating the (PISN) Mass Gap

From the full BH mass range (Figure 1), we extract sequential mergers with total mass within the mass gap, classify them in subregions (Figure 2), discuss their evolutionary pathways (Figure 3), and present their demographics (Figure 4 and Table 1).

#### 3.3.1. Red Subregion A

The predicted properties of systems in red subregion A are $M_{BBH,in} \ll M_{gap,max} \leqslant M_{BH,3}$ and $0.1 \lesssim \chi_{eff} \lesssim 0.27$. The evolution of an example system is illustrated in the top panel of Figure 3. Consider a CHE inner binary (triple type 1 or 2) with $M_1 \approx M_2 \approx 40\,M_\odot$, $R_1 \approx R_2 \approx 6\,R_\odot$, $a_{in} \gtrsim 18\,R_\odot$. All stars in this triple will experience complete fallback, which effectively leaves the inner and outer orbits unchanged (Section 2). Assuming the outer star collapses to a BH with mass $M_{BH,3} \approx 140\,M_\odot$, then $a_{out} \gtrsim (a_{out}/a_{in})|_{crit} \times a_{in} \approx 4.2 \times (18\,R_\odot) \approx 76\,R_\odot$ in order for the triple to be stable (Equation (1) and Figure 4). If the separation after the inner BBH merges is less than $a_{out,max} \lesssim 122\,R_\odot$, then the sequential merger can occur within a Hubble time (Equation (4)). The critical ratio of $a_{out}/a_{in}$ to maintain stability and the maximum orbital separation to achieve a merger within a Hubble time depend on the mass combinations of the triple and vary within a factor of a few for the combinations of interest here (Figure 4).

If the outer star was initially a standard evolving star (triple types 1 and 3), it might initiate a mass transfer phase onto the inner binary early in the evolution of the system (step A1 in Figure 3). This could occur if the radius of a standard evolving star exceeds the Roche lobe radius, i.e., $R_3 \gtrsim 0.43 \times a_{in}$ for $q_{out} \approx 140/80$. Assuming the stellar radii approach ~100–1000 $R_\odot$ at maximum (Podsiadlowski et al. 1992; Riley et al. 2020), tertiary-driven mass transfer occurs for outer orbits up to several ~100–1000 $R_\odot$.

During this mass transfer phase, where the tertiary donor is significantly heavier than the inner binary, the outer orbit likely

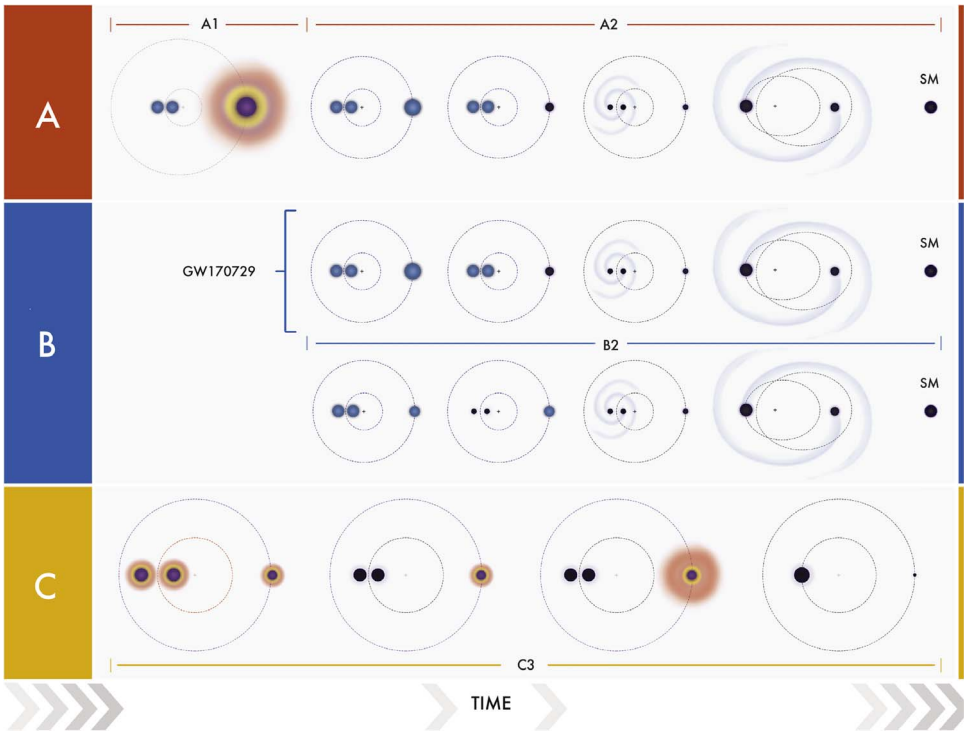


**Figure 3.** Time evolution of triple stellar systems. We illustrate compact stars in blue, standard evolving stars with red envelopes, BHs in black, and merging BBHs with a surrounding swirl. The BHs formed as sequential mergers are labeled SM. Architectures are described in Sections 3.1 and 3.2 and discussed in Section 3.3. Top: red subregion A, where the tertiary is the most massive star in the system and forms the first BH in this triple. The inner binary needs to be constituted of compact stars, and the tertiary can be either a standard evolving or compact star (triple types 1 and 2, respectively). Middle: blue subregion B, where all stars have similar masses. These triples can only lead to sequential mergers if all stars are compact (triple type 2). We suggest that GW170729 experienced this evolution. Bottom: yellow subregion C, where the tertiary is of significantly lower mass than either of the inner binary stars. We find that this configuration (triple type 3) does not lead to sequential mergers and is only presented for completion. Credit: T. Rebagliato.

shrinks (based on angular momentum considerations), and the hydrogen envelope is stripped off the outer star. If the inner binary avoids a merger during this stage (see, e.g., Leigh et al. 2020), at the end of the mass transfer phase, the tertiary is a stripped helium star reminiscent of the compact outer star considered in triple type 2.

In this section, so far we have considered inner binaries comprised of CHE stars that remain close to each other throughout their evolution to BBHs. However, for standard evolving inner binaries (triple types 3 and 4), the orbital separation can change drastically between the zero-age main sequence and BBH formation due to mass and angular momentum exchanges during mass transfer episodes. From our synthetic population, the orbits of standard evolving binaries can remain as small as $a_{\rm in} \approx 70\,{\rm R}_\odot$ throughout their evolution, but for most systems, their orbits expand to hundreds or thousands of solar radii (see, e.g., Leigh et al. 2020). Assuming the optimistic case of a standard evolving inner binary with $a_{\rm in} \approx 70\,{\rm R}_\odot$ maximally, the outer separation must be $a_{\rm out} \gtrsim 2.8 \times (70\,{\rm R}_\odot) \approx 196\,{\rm R}_\odot$ in order for the triple to be stable throughout its full evolution. Such an orbit does not merge by GW emission alone in a Hubble time (Figure 4). We conclude that in red subregion A, only triples with inner compact binaries can lead to sequential mergers within a Hubble time.

### 3.3.2. Blue Subregion B

The predicted properties of systems in blue subregion B are $M_{\rm BBH,in}/2 \approx M_{\rm BH,out} \leqslant M_{\rm gap,min}$ and $0.38 \lesssim \chi_{\rm eff} \lesssim 0.58$. The evolution of an example system is illustrated in the middle panel of Figure 3. Furthermore, the synthetic population suggests $M_{\rm BH,1} \approx M_{\rm BH,2}$ in this region; with similar BH masses, the evolutionary timescales for all component stars are similar as well. Consider a triple with $M_1 \approx M_2 \approx M_3 \approx 40\,M_\odot$. We again assume a CHE inner binary (triple type 1 or 2) with $R_1 \approx R_2 \approx 6\,{\rm R}_\odot$ and $a_{\rm in} \gtrsim 18\,{\rm R}_\odot$. This triple is dynamically stable if $a_{\rm out} \gtrsim 3.3 \times (18\,{\rm R}_\odot) \approx 60\,{\rm R}_\odot$. The outer separation must be $a_{\rm max} \lesssim 76\,{\rm R}_\odot$ for the sequential merger to occur within a Hubble time due to GW emission. Hence, the small possible range for outer separations of $60 \lesssim a_{\rm out}/{\rm R}_\odot \lesssim 76$ constrains the feasibility and frequency of this subchannel. Population III BBH progenitors with initial masses $M_1 \gtrsim 40\,M_\odot$ and $q \approx 1$ have initial separations $a_{\rm in} \gtrsim 20\,{\rm R}_\odot$ (Inayoshi et al. 2017), which lead to slightly more stringent constraints than for CHE binaries.

If the tertiary was a standard evolving star (triple types 1 and 3), it could initiate a mass transfer episode onto the inner binary. Due to the mass ratio, we expect this mass transfer to proceed in a stable manner. Furthermore, we expect the outer orbit to widen, typically due to angular momentum evolution, which makes the sequential merger less likely to occur within a Hubble time (see, e.g., Belczynski et al. 2002, for an overview in the context of BBH progenitors). In summary, in blue subregion B, only triple compact binaries in a fine-tuned configuration can lead to sequential mergers within a Hubble time.

### 3.3.3. Yellow Subregion C

The masses of systems in yellow subregion C are $M_{\rm BH,3} \ll M_{\rm gap,max} \leqslant M_{\rm BBH,in}$. The evolution of an example system is illustrated in the bottom panel of Figure 3. Even though our synthetic binary population does not predict any inner BBHs in this region (Appendix), BBHs above the mass gap have been suggested for both compact (Marchant et al. 2016;

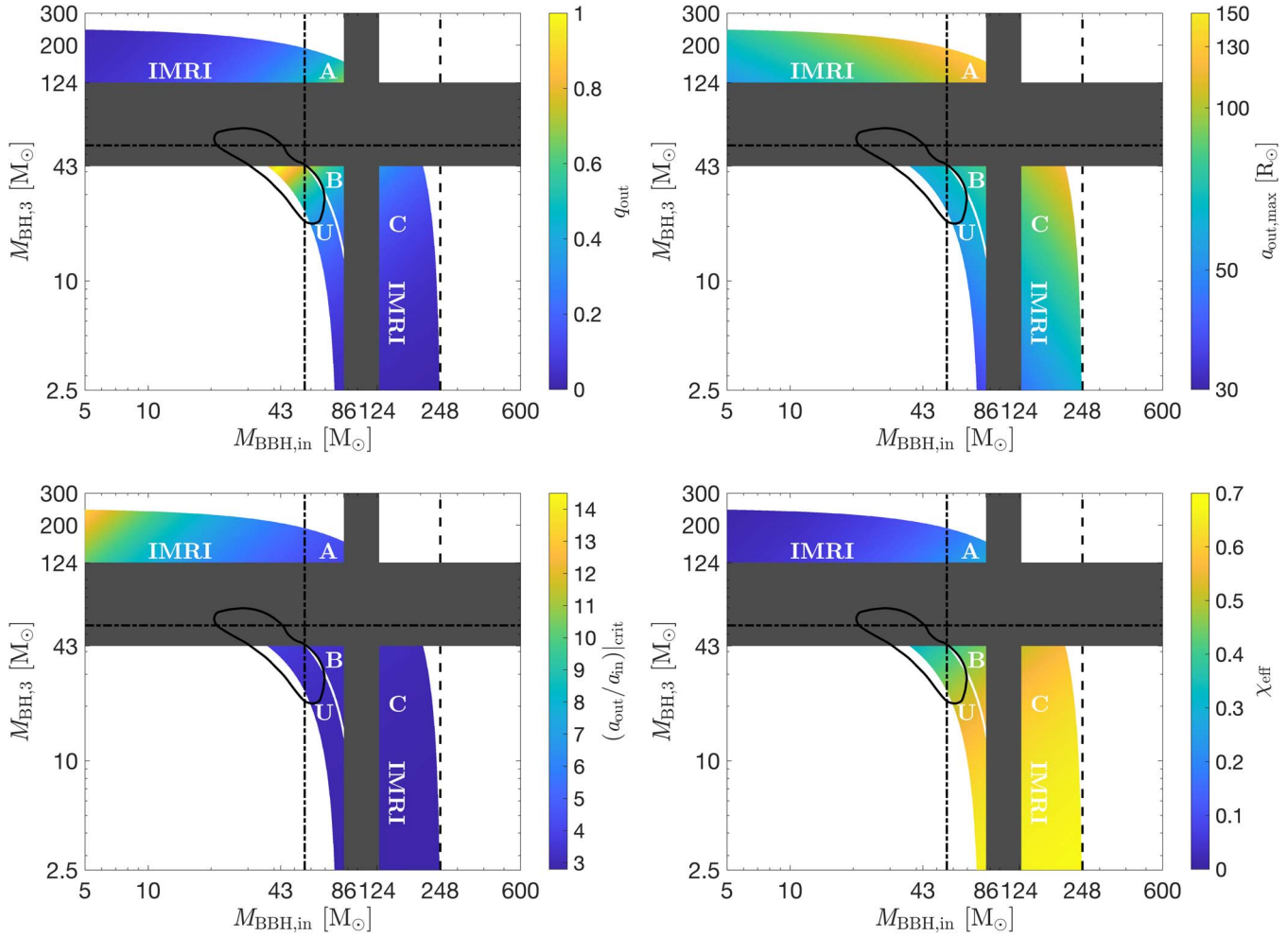


**Figure 4.** Overview of mass combinations for isolated triples leading to sequential mergers with total mass in the (PISN) mass gap (see captions of Figures 1 and 2 for additional details). The color in each panel denotes a different physical property. The 90% confidence intervals for GW170729 (Chatziioannou et al. 2019) are shown as a solid black line. Top-left panel: outer mass ratio ($q_{\rm out}$) for the sequential merger. Top-right panel: maximum separation in which a circular binary with component masses $M_{\rm BBH,in}$ and $M_{\rm BH,3}$ can merge within the age of the universe due to GW emission. Bottom-left panel: minimum ratio of outer and inner orbital separation for dynamical stability, assuming a circular coplanar prograde orbit. Bottom-right panel: effective dimensionless spin ($\chi_{\rm eff}$) of the sequential merger, assuming coplanarity in the inner and outer orbit. Note that $\chi_{\rm eff} > 0$ and ≈0.4 for LIGO Scientific Collaboration and the Virgo Scientific Collaboration (LVC)-like sources (around subregion B).

**Table 1**
Summary of Expected Demographics of Different Types of Sequential Mergers

| Region | A-IMRI | A | U | B | C-IMRI |
|---|---|---|---|---|---|
| Rank | 4 | 2 | 1 | 3 | 5 |
| Region | Red | Red | Blue | Blue | Yellow |
| Triple type | 1 | 1 and 2 | 1 and 2 | 1 and 2 | 3 |
| Mass gap $M_{\rm BBH,in}$ | No | Yes | Uncertain | Yes | No |
| $M_{\rm BH,3}$ | [124, 243] | [124, 205] | [2.5, 43] | [14, 43] | [2.5, 43] |
| $M_{\rm BBH,in}$ | [5, 43] | [43, 86] | [37, 86] | [57, 86] | [126.5, 245.5] |
| $M_{\rm BH,3} + M_{\rm BBH,in}$ | [129, 248] | [167, 248] | [80, 100] | [100, 129] | [129, 248] |
| $q_{\rm out}$ | [0, 0.1] | [0.1, 0.69] | [0, 1] | [0.16, 0.74] | [0, 0.1] |
| $a_{\rm out}$ | [52, 120] | [97, 135] | [35, 69] | [57, 82] | [45, 120] |
| $\chi_{\rm eff}$ | [0, 0.1] | [0.1, 0.27] | [0.4, 0.68] | [0.38, 0.58] | [0.5, 0.68] |
| $(a_{\rm out}/a_{\rm in})\vert_{\rm crit}$ | [4.8, 13.3] | [4.0, 5.7] | [2.8, 3.8] | [3.0, 3.3] | [2.8, 3.1] |

**Note.** This table summarizes the results from Section 3 and all figures. For each quantity of interest, we present the minimum and maximum values in square brackets. We have subjectively provided a ranking for the most (1) to least (5) likely scenario to form a sequential merger based on the inner BBH mass distribution, the condition for triple stability, and the sequential merger time. Masses and separations are in solar units.

du Buisson et al. 2020) and standard evolving (Mangiagli et al. 2019) binaries. Regarding the former, as inner binaries experiencing CHE (triple types 1 or 2) are expected to have mass ratios $q_{\rm in} \approx 1$ and $M_{\rm BBH,in} \gtrsim 2 \times M_{\rm gap,max} \approx 248\ M_\odot$, these systems can only bring about sequential mergers with a total mass above the mass gap. Regarding the latter, the case of hypothetical

standard evolving binaries is also not promising for sequential mergers. If mass transfer took place from the lower-mass tertiary companion to the heavier-mass inner binary, it would likely be stable and widen the outer orbit. This would increase the GW inspiral time for the outer orbit. Therefore, we do not consider sequential mergers from subregion C to be common.

### 3.4. GW170729 as a Sequential Merger

With a reported chirp mass $\mathcal{M} = (M_1 M_2)^{3/5}/(M_1 + M_2)^{1/5} = 35.4^{+6.5}_{-4.8}\,M_\odot$, postmerger remnant BH mass of $79.5^{+14.7}_{-10.2}\,M_\odot$, $\chi_{\rm eff} = 0.37^{+21}_{-25}$, and redshift $z = 0.49^{+0.19}_{-0.21}$ (Abbott et al. 2019), GW170729 can be marginally considered in the mass gap (Figures 1, 2, and 4). While Rodriguez et al. (2019) associated GW170729 with a cluster origin, Kimball et al. (2020) claimed a standard stellar evolution origin. Here we propose that the heavier BH of GW170729, with an inferred mass of $50.2^{+16.2}_{-10.2}\,M_\odot$, is the remnant of an inner BBH from a sequential merger.

The scenario we suggest is the following. We consider a CHE system (triple type 3) at metallicity $Z = 10^{-4}$ with an inner overcontact binary of $M_1 = M_2 = 29\,M_\odot$, $R_1 = R_2 \approx 4.8\,R_\odot$, and $a_{\rm in} \approx 10.5\,R_\odot$ and a tertiary companion with $M_3 = 33.5\,M_\odot$, $a_{\rm out} = 43.5\,R_\odot$, and $e_{\rm out} = 0$. This satisfies the stability condition for the triple as $a_{\rm out} > 3.4 \times (10.5\,R_\odot) \approx 35\,R_\odot$ (Figure 4). At that time, the outer orbit has a relative speed of $\sqrt{G(M_1 + M_2 + M_3)/a_{\rm out}} \approx 600$ km s$^{-1}$. All stars in this triple will experience complete fallback and negligible stellar winds, which effectively leave the inner and outer orbits unchanged. The only mass change during BH formation comes from the relation between baryonic and gravitational mass (Fryer et al. 2012). The first star to collapse to an $\approx 30.2\,M_\odot$ BH is the tertiary at around 6 Myr. Subsequently, the inner binary evolves into an $\approx 26 + 26\,M_\odot$ BBH at around 7 Myr. Afterward, evolution is purely driven by GW radiation. It takes the inner binary $\sim$50 Myr to merge and form a single BH with $M_{\rm BBH,in} \approx (1 - f_{\rm rad})(M_{\rm BH,1} + M_{\rm BH,2}) \approx 49.5\,M_\odot$, spin $|\chi_{\rm BBH,in}| = 0.68$ (Boyle et al. 2008), separation $a_{\rm out} \approx 45\,R_\odot$ (Equation (2)), and $e_{\rm out} \approx 0$ (Equation (3)). After $\sim$5.1 Gyr (Equation (4)), the second merger takes place. This sequential merger has a chirp mass of $\approx 33.5\,M_\odot$, $\chi_{\rm eff} \approx 0.4$ (Figure 4), and $z \approx 0.49$ (see Appendix C for redshift calculation and details on the evolution) and is shown in Figures 1 and 2 as a diamond (Triple-SM).

### 3.5. GW190521: A BBH in the Mass Gap

The inferred total mass of GW190521 is within the mass gap with BH component masses of $85^{+21}_{-14}$ and $66^{+17}_{-18}\,M_\odot$ (Abbott et al. 2020a, 2020b). The heavier BH of GW190521 has a mass greater than $60\,M_\odot$ (Fishbach & Holz 2020) and therefore cannot be easily associated with isolated binaries (Section 4.3). While uncertainties in the inferred component masses make it tempting to associate GW190521 with a triple origin, the inferred spins suggest otherwise. The high individual spins ($|\chi_{1,2}| > 0.69$) and low effective spin ($\chi_{\rm eff} \approx 0$) imply that BH spins are not aligned with the orbit (Equation (5)). We conclude that GW190521 is inconsistent with our predictions of sequential mergers.

## 4. Discussion

### 4.1. Main Caveats to Our Method

The main caveats of the scheme presented in this Letter are the natal properties of BHs and the assumed orbital distributions (Section 4.2). The remnant masses, birth spins, and natal kicks of BHs remain an open question in astrophysics. The assumption of low (Population II and III) metallicity and complete fallback make mass loss and natal kicks negligible (Fryer et al. 2012; Müller et al. 2016). This is favorable for sequential mergers because any potential widening of the inner orbit can trigger a dynamical instability of the triple and increase the GW inspiral time. However, some models of CHE binaries predict that Wolf–Rayet mass loss is nonnegligible (e.g., Marchant et al. 2016). Complete fallback is less likely for BH progenitors with carbon–oxygen masses $\lesssim 11\,M_\odot$ (Fryer et al. 2012), some of which are associated with GW sources (see, e.g., GW170608 from Abbott et al. 2019).

Natal kicks could tilt the orbital spins, change eccentricities, and induce inclinations, modifying the evolution from the moment the first BH is born. In some cases, the direction and magnitude of the kick could decrease the inner BBH merger timescale; in others, it could ionize the triple before the sequential merger (other effects discussed in Section 4.2). The extreme case of natal kicks with velocities $\gtrsim 100$ km s$^{-1}$ could even disrupt the system at BH formation.

The spin transition from star to BH is also quite uncertain. Recent studies suggest that angular momentum transport (Fuller & Ma 2019) and accretion feedback (Batta & Ramirez-Ruiz 2019) disfavor maximally spinning BHs. While most BHs are probably born with low spins, CHE can lead to moderate and even high spins (Fuller & Ma 2019). Spin alignment with the orbital angular momentum vector (e.g., CHE binaries) prevents a GW recoil kick even for maximally spinning BHs. Moderate and high misaligned spins can lead to GW recoil kicks of tens or hundreds of kilometers per second (Lousto et al. 2010). These kicks would not necessarily disrupt our systems (e.g., Section 3.4).

We assume no rotation at birth in order to establish lower limits on effective spins but remain agnostic on what a realistic natal BH kick and spin distribution should be.

### 4.2. Stellar Triples: Birth Distributions and Orbital Evolution

The expected rate of sequential mergers depends on the abundance of massive triples and their architectures. Even though these are unconstrained at low metallicities, observations in the Local Group indicate that for O-type stars in the range $16 \leqslant M/M_\odot \leqslant 40$, the triple multiplicity fraction is $\approx$0.35 (Moe & Di Stefano 2017). Multiplicity in massive stars affects the evolutionary outcomes of field systems, and isolated binary, triple, and quadruple evolution jointly contribute to, e.g., the double compact object merger rate.

Close observed systems ($P_{\rm orb} \lesssim 1$ au) are preferably circular (Sana et al. 2012; Moe & Di Stefano 2017). Observations of tight ($\lesssim$50 au) low-mass and intermediate-mass ($\lesssim 4\,M_\odot$) triples show a strong tendency toward orbital alignment ($\lesssim 36°$) and are therefore likely to avoid Lidov–Kozai cycles (Tokovinin 2017). However, the orbital distributions of massive stellar triples are yet unknown. Diverging from our simplified assumption of circular coplanar prograde orbits might abruptly modify the evolution of the BH triple due to three-body dynamics. This would induce high(er) eccentricities (Naoz 2016) in the inner binary that may lead to exchanges of mass, mergers (Iben & Tutukov 1999; Moe & Di Stefano 2017), and disruptions (e.g., He & Petrovich 2018). Additionally, mass transfer initiated from the tertiary could have the gaseous envelope change the characteristics of the inner binaries with respect to our adopted synthetic population (de Vries et al. 2014). It may even provoke

a merger of the inner binary and provide an electromagnetic counterpart (Leigh et al. 2020). In general, mergers between the two stars of a triple can lead to different systems than the ones expected from pristine binaries (e.g., Podsiadlowski et al. 1992; Vigna-Gómez et al. 2019). It is therefore likely that triples play a nonnegligible role in massive stellar evolution.

Eccentricity of the outer orbit is an additional caveat. While the GW coalescence timescale is significantly shorter for eccentric binaries (Peters 1964), the minimum ratio of $a_{\rm out}/a_{\rm in}$ to guarantee dynamical stability is larger for more eccentric systems (Mardling & Aarseth 2001). Both of these directly affect the number of sequential mergers.

Future observations of massive stars will shed light on the orbital birth distributions of triples. This will help to validate our assumptions and constrain the rates of sequential mergers.

### 4.3. Uncertainties in the (PISN) Mass Gap

The exact location and existence of the mass gap is an open question (see, e.g., Belczynski 2020, and references therein). Any model uncertainties on the limits of the mass gap directly propagate to the predicted BBH mass distribution of sequential mergers. Metal-free (Population III) stars, which can be compact and are believed to lead to more massive BH progenitors, have been suggested to shift the edge of the mass gap (e.g., Farrell et al. 2020; Tanikawa et al. 2020). Helium stellar models predict that the location of the lower edge of the mass gap is robust against variations in (Population II) metallicity, treatment of rotational mixing, and wind mass loss but sensitive to nuclear reaction rates giving $40 \lesssim M_{\rm gap,min}/M_\odot \lesssim 56$ (Farmer et al. 2019). Variation on the $^{12}{\rm C}(\alpha,\gamma)^{16}{\rm O}$ rate could shift the limit to $M_{\rm gap,min}/M_\odot \lesssim 56$–90 (Farmer et al. 2020) and even make the mass gap disappear (Costa et al. 2020). Different supernova prescriptions lead to an uncertainty in the range $40 \lesssim M_{\rm gap,min}/M_\odot \lesssim 50$ (Stevenson et al. 2019). Mass transfer in binaries does not significantly affect the location of the mass gap (van Son et al. 2020). The GW sources are an exciting prospect to study the mass gap, with the caveat that they must first be segregated into field or cluster origin.

### 4.4. Multiple BH Mergers

Mass gap mergers are usually associated with multiple BH mergers in clusters (e.g., GW190521, as discussed in Abbott et al. 2020b, and references therein). Such mergers are expected to occur readily when central densities are high (Samsing & Hotokezaka 2020). Multiple BH mergers lead to effective spins in the range $-0.5 \lesssim \chi_{\rm eff} \lesssim 0.5$ (Rodriguez et al. 2019). The rates of multiple BH mergers decrease significantly for spinning BHs, as their merger experiences a recoil kick of magnitude comparable to or larger than the escape speed of the cluster (Rodriguez et al. 2019). On the other hand, a massive stellar field triple is less likely to be disrupted during the inner BBH merger (Section 2). A pileup of GW sources in the mass gap with $\chi_{\rm eff} \gg 0$ could be indicative of isolated triple origin. Additionally, systems in which both BHs have masses above the mass gap and $\chi_{\rm eff} < 0$ should be seriously considered of cluster origin.

Multiple stellar systems have also been associated with BBH mergers. Standard evolving hierarchical triples of field or cluster origin can lead to an inner BBH merger by perturbations of the third companion (Fragione & Kocsis 2020; Martinez et al. 2020). Standard evolving quadruple systems have also been suggested as progenitors of BBH mergers. Some of them can be composed of two BBH binaries, where the recoil kick of the merger remnant of one BBH triggers the interaction with the other BBH, likely exchanging a component and eventually leading to a BBH merger (Fragione et al. 2020). Others can be hierarchical quadruples, where the Lidov–Kozai effect assists in the sequential merger of the two inner binaries (Safarzadeh et al. 2020).

Alternatively, some BBHs orbiting around galactic nuclei can experience Lidov–Kozai perturbations from the central supermassive BH, increasing the BBH merger rate (Hoang et al. 2018).

### 4.5. Intermediate Mass-ratio Inspirals

Sequential mergers with $M_{\rm BBH,in} > 100$ and $M_{\rm BH,3} < 43\,M_\odot$, which correspond to the red and yellow regions above the mass gap in Figures 1 and 2, are intermediate mass-ratio inspirals (IMRIs) and can be degenerate with those of binary origin (Appendix D). The BHs with $M_{\rm BH} \gtrsim 100\,M_\odot$ are usually associated with clusters (see Miller & Colbert 2004, for a review) but can also be formed by single massive stars (Heger et al. 2003). No IMRIs have yet been detected, but the merger product of GW190521 is the first detected intermediate-mass BH (Abbott et al. 2020a).

For our assumptions, we expect $\chi_{\rm eff} = 0$ for the IMRIs of binary origin; therefore, $\chi_{\rm eff} \gg 0$ is a strong indicator of sequential merger origin. The IMRIs in the yellow region have $0.5 \lesssim \chi_{\rm eff} \lesssim 0.68$, but those in the red region have $0 \lesssim \chi_{\rm eff} \lesssim 0.1$ (Figures 1, 2, and 4 and Table 1).

### 4.6. Rate of Sequential Mergers

At redshift $z = 0$, Riley et al. (2020) predicted a BBH merger rate of $50\,{\rm Gpc^{-3}\,yr^{-1}}$, which we use to estimate a sequential merger rate $\mathcal{R} < 3\ {\rm Gpc^{-3}\ yr^{-1}}$ from field triples (Appendix E), similar to the estimated rate from hierarchical triples in clusters (Martinez et al. 2020) and the field (Antonini et al. 2017).

For sequential mergers, the inner compact BBH is likely a fast merger ($\lesssim$100 Myr), while the wide outer orbit merges in longer timescales (∼gigayears; Figure 4). This hierarchical nature leads to a cutoff in the delay time distribution at early times and a possible pileup at higher redshifts, which can be probed with third-generation GW detectors (Abbott et al. 2017). It is further supported by the fact that lower-metallicity environments are believed to dominate at higher redshifts.

## 5. Conclusions

We investigated configurations of isolated massive stellar triples that lead to sequential BBH mergers. We find that triples with CHE inner binaries are good candidates for sequential mergers. Our model predicts that GW sources with one BH in the mass gap and $\chi_{\rm eff} > 0.1$ can be of sequential merger origin. We highlight two classes of triples that lead to BBHs in the mass gap. The first one has a tertiary BH above the mass gap and $0.1 \lesssim \chi_{\rm eff} \lesssim 0.27$ (see red subregion A in Figures 2 and 4). The second one has a tertiary BH below the mass gap and $0.38 \lesssim \chi_{\rm eff} \lesssim 0.58$ (see blue subregion B in Figures 2 and 4). We suggest that GW170729 is of triple origin and belongs to the second class. The masses and spins of mass gap event GW190521 are inconsistent with our model, which further supports a cluster origin.

From a broader point of view, we outlined a new outcome of the evolution of massive stellar triples from a proof-of-principle study. To improve upon the predictions made here, several processes should be considered: the effects of the uncertain initial orbital configurations of stellar triples, which may also lead to nonnegligible three-body dynamical effects; the nontrivial problem of mass transfer in triples; GW recoil kicks from the inner BBH merger; and their combined effects on population statistics. Higher-order multiplicity in massive stars is crucial to understanding the most energetic astronomical phenomena in the Universe.

The authors thank David R. Aguilera-Dena, Chris Belczynski, Giacomo Fragione, Ryosuke Hirai, Ilya Mandel, Chris Moore, Ataru Tanikawa, and Team COMPAS for useful discussions and suggestions. We thank Teresa Rebagliato for the graphic representation of the formation channels. A.V.-G. and E.R.-R. acknowledge funding support by the Danish National Research Foundation (DNRF132). E.R.-R. is also supported by the Heising-Simons Foundation and NSF (AST-1911206 and AST-1852393). S.T. acknowledges support from the Netherlands Research Council NWO (VENI 639.041.645 grants). N.W.C.L. gratefully acknowledges support from the Chilean government via Fondecyt Iniciación grant No. 11180005. C.-J.H. acknowledges the support of the National Science Foundation and the LIGO Laboratory. LIGO was constructed by the California Institute of Technology and Massachusetts Institute of Technology with funding from the National Science Foundation and operates under cooperative agreement PHY-1764464.

*Software:* COMPAS[11] v02.11.04, publicly available at GitHub via TeamCOMPAS/COMPAS.[12] Scripts used for this study are available in GitHub via avigna/sequential-mergers.[13]

## Appendix A
## Rapid Population Synthesis

We use the publicly available data from Riley et al. (2020) for synthetic BBH formation and merger rates. That study made use of the COMPAS rapid population synthesis code (Stevenson et al. 2017; Vigna-Gómez et al. 2018; Neijssel et al. 2019), which is freely available at http://github.com/TeamCOMPAS/COMPAS. The version of COMPAS used for these simulations was v02.11.01a, built specifically for Riley et al. (2020); functionality in this release was integrated into the public COMPAS code base in v02.11.04.

Riley et al. (2020) performed, for the first time, simultaneous population synthesis of CHE and standard evolving binaries. We use the orbital distributions of BBH mergers from that study as an educated guess for the properties of the inner BBH in the sequential merger scenario. While this works well as a first approach, the initial conditions from Riley et al. (2020) are based on birth distributions from observations of isolated massive binaries (Sana et al. 2012). Riley et al. (2020) simulated binaries with metallicities $-4 \leqslant \log_{10} Z \leqslant -1.825$. As there are no binary evolution models available at zero-metallicity Population III stars, all of our quantitative results from compact binaries come exclusively from CHE binaries.

The most relevant conclusions drawn from this data concerning sequential mergers are as follows.

1. There are, overall, $\sim 4\times$ more merging BBHs from standard evolving than from CHE binaries. The local merger rate ($z = 0$), which accounts for star formation history and galaxy mass–metallicity dependence, is 50 and 20 $\mathrm{Gpc}^{-3}\ \mathrm{yr}^{-1}$ for isolated binaries and the subset of CHE binaries, respectively. For CHE binaries, we include massive overcontact binaries. A massive overcontact binary can fill its inner Lagrangian point during the main sequence as long as the outer Lagrangian point is not filled (Marchant et al. 2016).
2. The yield of merging BBHs from CHE binaries is roughly constant below $\log_{10} Z/Z_\odot \lesssim -0.5$ (see Figure 6 of Riley et al. 2020), with $Z_\odot = 0.0142$. Low-metallicity CHE stars are more compact than high-metallicity ones; they also experience less mass loss and orbital widening through stellar winds.
3. The maximum premerger total mass of BBHs for both CHE and standard evolving binaries is $M_{\mathrm{BH},1} + M_{\mathrm{BH},2} \approx 79\, M_\odot$.
4. In this COMPAS data set, there are no BBHs above the mass gap. This holds even when including stars with initial masses up to 150 $M_\odot$, for which the adopted stellar evolution models from Hurley et al. (2000) are extrapolated to stars above 50 $M_\odot$. However, we consider that there is a possibility of BBHs above the mass gap in nature. They could come from standard evolving stars (e.g., Mangiagli et al. 2019) or CHE binaries (e.g., Marchant et al. 2016; du Buisson et al. 2020).
5. We use the *delayed* supernova mechanism prescription from Fryer et al. (2012) to determine the remnant mass and natal kick distributions. This prescription predicts complete fallback for BH progenitors with carbon–oxygen core masses above 11 $M_\odot$. In our population, more than half of standard evolving stars and all CHE stars leading to BBHs have masses above this threshold. Complete fallback has two implications. The first is that the final baryonic mass of the remnant is the same as the presupernova mass (Equations (19) and (20) from Fryer et al. 2012) modulo neutrino emission. The second is that there are no natal kicks for heavy BHs (Equation (21) of Fryer et al. 2012).

We emphasize that a full population synthesis of massive stellar triples will help us better understand the evolution of sequential mergers and their delay time distribution and constrain their rates. We hope future software developments and observations will make this sort of study possible in the near future.

## Appendix B
## Radiated Mass during BBH Mergers

For a BBH, $f_{\mathrm{rad}}$ is the amount of energy radiated away in the form of GWs during the coalescence, expressed as a fraction of the total mass of the BBH. While the magnitude of $f_{\mathrm{rad}}$ is independent of the BBH total mass, it does depend on the binary mass ratio $q_{\mathrm{in}} = M_{\mathrm{BH},2}/M_{\mathrm{BH},1}$ (with $M_{\mathrm{BH},1} \geqslant M_{\mathrm{BH},2}$) and the BH spin configuration. More specifically, it depends on $\chi_{1,2}^{L^{\parallel}} \equiv \chi_{1,2}\cos(\theta_{1,2})$, with $0 \leqslant \chi_{1,2} \leqslant 1$ being the BH spin magnitude and $\theta_{1,2}$ the zenith angle between the spin and orbital angular momenta at the time of merger for each BH. The $f_{\mathrm{rad}}$ is typically approximated by making use of fitting

[12] https://github.com/TeamCOMPAS/COMPAS
[13] https://github.com/avigna/sequential-mergers

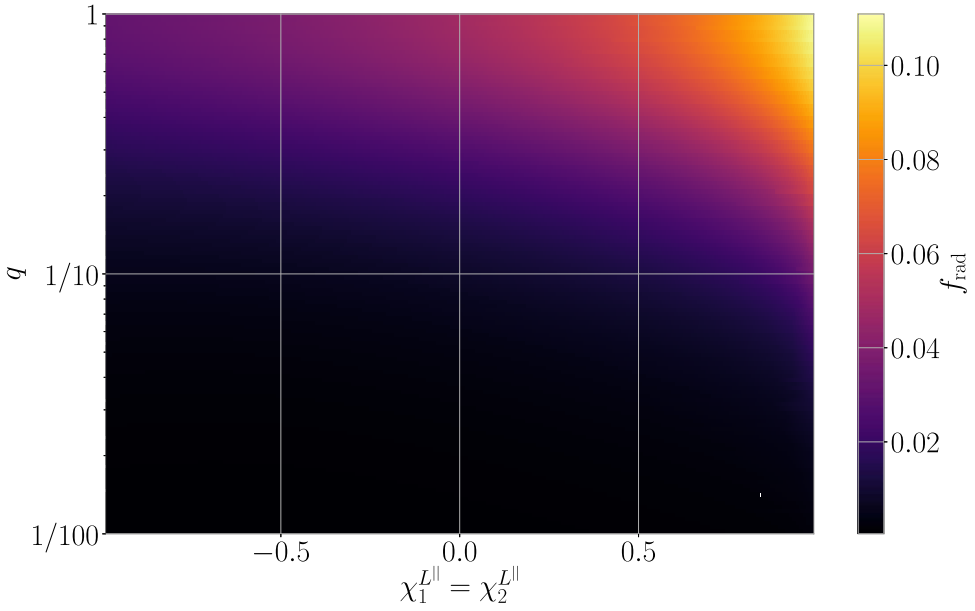


**Figure 5.** Radiated mass fraction, $f_{\rm rad}$, from a BBH merger. For simplicity, we present the case for equal spins aligned with the orbital angular momentum vector $\hat{L}_{\rm N}$. In this Letter, we focus on the nonrotating scenario with $\chi_{1,2}^{L\|} = 0$. We use this to estimate the GW Blaauw kick of the inner BBH merger in Section 2.

formulae that are based on numerical relativity simulations of BBHs.

In this study, we use the prescription from Equation (28) of Jiménez-Forteza et al. (2017) as implemented in LALSuite (LIGO Scientific Collaboration 2018) and show $f_{\rm rad}$ for a selection of BH spins and mass ratios in Figure 5. For simplicity, and following our assumptions, we have restricted the figure to binaries with equal $\chi_{1,2}^{L\|}$ values. We use this prescription to estimate the final masses from both the inner BBH merger (Figures 1 and 2) and sequential mergers.

## Appendix C
## Redshift Estimate

In order to test the validity of the sequential merger scenario for Abbott et al. (2019), we focus on the expected delay times for our scenario. The delay time is the time it takes a system to evolve from the zero-age main sequence to the sequential BBH merger and follows from our models. We will convert it into a redshift in the following way. We use `astropy's cosmology` module to convert between redshift and look-back time using `astropys lookback_time` (Astropy Collaboration et al. 2013, 2018). We assume a flat ΛCDM cosmology with $H_0 = 67.90\,{\rm km\,s^{-1}\,Mpc^{-1}}$ and $\Omega_{\rm m} = 0.3065$ following Planck Collaboration et al. (2016). With this setup, for a delay time of ∼5.1 Gyr, we estimate a redshift $z \approx 0.49$.

## Appendix D
## IMRIs

In Figure 2, we mark the region of sequential mergers with masses $M \geqslant 124\,M_\odot$ and mass ratios $q < 0.2$ as being IMRIs. This type of system is degenerate with IMRIs of binary origin. The IMRIs have primary masses of, e.g., $M_{\rm BH,1} \geqslant 100\,M_\odot$ and mass ratios of, e.g., $q < 0.1$ (see, e.g., Haster et al. 2016a, 2016b). In Section 4.5, we briefly discuss how they are usually associated with a cluster origin, but we do not rule out an isolated origin. In Table 1, we present the properties of IMRIs from red subregion A and yellow subregion C.

In this Appendix, we briefly expand our analysis of sequential mergers leading to systems that are degenerate in mass with IMRIs. Figure 6 considers double compact objects with primary masses $124 \leqslant M_{\rm BH,1}/M_\odot \leqslant 500$ and light compact object masses $1 \leqslant M_{\rm light}/M_\odot \leqslant 43$. In this case, light compact objects include both neutron stars and BHs. It is not dependent on the maximum mass of neutron stars or the existence or absence of a mass gap between neutron stars and BHs. These limits constrain the mass ratio to $0 \lesssim q \lesssim 0.35$. To date, GW190814 is the GW source with the most extreme mass ratio of $q = M_{\rm light}/M_{\rm BH,1} \approx 2.6/23 \approx 0.11$ (Abbott et al. 2020c). However, the individual masses of GW190814 are well below those of typical IMRIs.

For an IMRI, the inference of the effective spin might not be enough to classify its origin. For a sequential merger, if the tertiary is the most massive component, then the effective spin is dominated by this massive nonrotating BH, i.e., $\chi_{\rm eff} \approx 0$. This value would be similar to that of a nonrotating binary. On the other hand, if the tertiary is the least massive component, that effective spin is $\chi_{\rm eff} \approx 0.7$. This is summarized visually in Figure 4 and quantitatively in Table 1.

More detailed studies of the spin properties of BBH mergers from isolated binary, isolated triple, and cluster origin would help in the classification of future detections of IMRIs. Additionally, population studies might be helpful in constraining the merger rates from different formation channels.

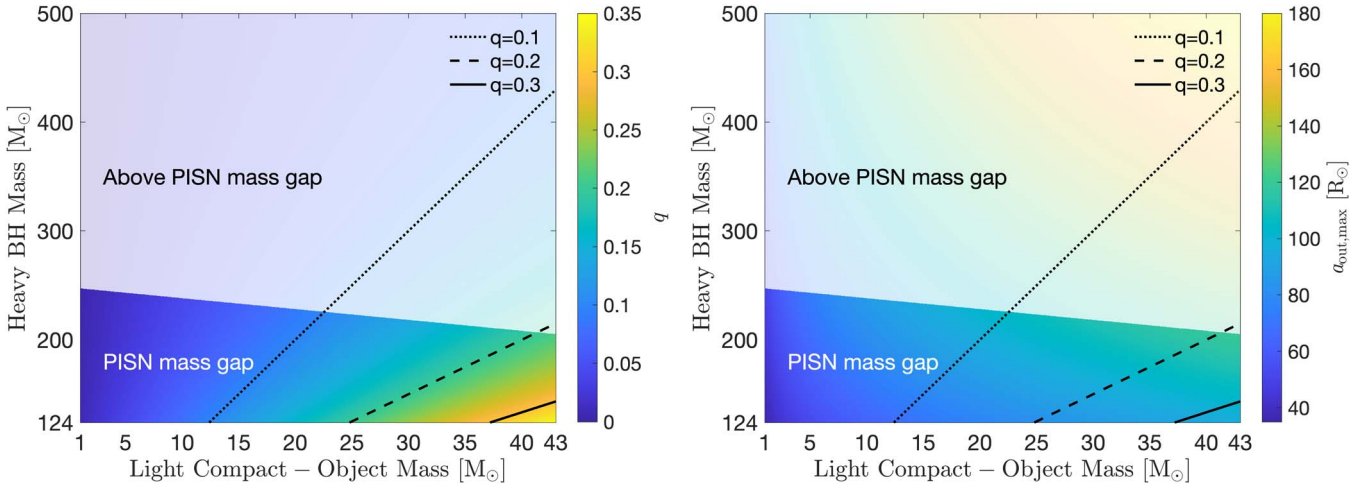


**Figure 6.** The IMRI systems can populate the mass gap as binaries in the total mass parameter space, but if their component masses are properly resolved, they can be excluded. The transparency shows the region outside the mass gap. This plot is similar to the red region from Figure 1 in the limit where $M_{\mathrm{BH},2} \ll M_{\mathrm{BH},1}$.

## Appendix E
## Sequential Merger Rate Estimate

In order to give an upper limit in the local ($z = 0$) rate of sequential mergers ($\mathcal{R}$), we make a simple estimate in the form

$$\mathcal{R} = \mathcal{R}_{\mathrm{BBH,in}} \times (f_{\mathrm{triple}}/f_{\mathrm{binary}}) \times f_{\mathrm{separation}}. \quad \text{(E1)}$$

We estimate the BBH merger rate $\mathcal{R}_{\mathrm{BBH,in}} = 50\ \mathrm{Gpc^{-3}\ yr^{-1}}$ based on the isolated binary evolution calculations of Riley et al. (2020), which account for both compact and standard evolving stars. This optimistic rate includes sequential mergers with a total mass below the mass gap. Riley et al. (2020) assumed that a fraction $f_{\mathrm{binary}} = 0.7$ of massive star systems are binaries. The factor $f_{\mathrm{triple}} = 0.35$ describes the fraction of massive star systems that are stellar triples (Moe & Di Stefano 2017).

The factor $f_{\mathrm{separation}}$ accounts for the fraction of systems in which the outer orbital can merge within a Hubble time due to GW emission. To estimate $f_{\mathrm{separation}}$, we assume that the log of the outer birth orbital separation is distributed uniformly $p(a_{\mathrm{out}}) \propto a_{\mathrm{out}}^{-1}$ (Öpik 1924; Abt 1983). We then estimate the fraction of systems of interest in the form

$$f_{\mathrm{separation}} = \frac{\int_{a_{\mathrm{out-SM,min}}}^{a_{\mathrm{out-SM,max}}} a^{-1} da}{\int_{a_{\mathrm{out,min}}}^{a_{\mathrm{out,max}}} a^{-1} da} = \frac{\int_{35\,\mathrm{R}_\odot}^{135\,\mathrm{R}_\odot} a^{-1} da}{\int_{28\,\mathrm{R}_\odot}^{2\times10^6\,\mathrm{R}_\odot} a^{-1} da} \approx 0.12, \quad \text{(E2)}$$

where $a_{\mathrm{out}}$ is the outer separation of stable triples, and $a_{\mathrm{out\text{-}SM}}$ is the outer separation of potential sequential mergers. The lower limit on $a_{\mathrm{out}}$ is given by the smallest value for a stable triple with an inner binary separation $a_{\mathrm{in}} \approx 10\,\mathrm{R}_\odot$, $(a_{\mathrm{out}}/a_{\mathrm{in}})_{\mathrm{crit}} = 2.8$, and therefore $a_{\mathrm{out,min}} = 28\,\mathrm{R}_\odot$. The maximum outer separation at birth that we consider is $a_{\mathrm{out,max}} \approx 10^4$ au $\approx 2 \times 10^6\,\mathrm{R}_\odot$ (Moe & Di Stefano 2017). For the outer separation of potential sequential mergers, following the results of Table 1, as shown in top right panel of Figure 4, the limits are $35 \lesssim a_{\mathrm{out\text{-}SM}}/\mathrm{R}_\odot \lesssim 135$. These limits in $a_{\mathrm{out\text{-}SM}}$ assume that the separation does not drastically change from the zero-age main sequence until the inner BBH merger. For some triples, this assumption will not necessarily hold (Section 4). When it holds, we expect the distribution of merger times to be $p(t) \propto t^{-1}$, as expected from GW-dominated binaries with a flat-in-the-log distribution at BBH formation. This assumption also neglects initially wider tertiary stars that are stripped and become potential sequential mergers (Section 3.3.1), which would increase the values of $a_{\mathrm{out\text{-}SM,max}}$, $f_{\mathrm{separation}}$, and, ultimately, the rate. The assumption of different orbital initial distributions would naturally also affect the rates. We choose these assumptions for an order-of-magnitude estimate and leave a more thorough analysis of the orbital parameter space and the distribution of merger times for a future study.

After substituting all of the estimated parameters in Equation (E1), we constrain the upper limit to $\mathcal{R} < 3\ \mathrm{Gpc^{-3}\ yr^{-1}}$ for sequential mergers.

## Appendix F
## More Details on the Evolution of GW170729

As a proof of concept of the evolution toward sequential mergers, we have simulated the evolution of the proposed progenitor of GW170729 with two independent codes: the rapid binary population synthesis code COMPAS and the triple evolution code TRES (Toonen et al. 2016, 2020). We use these codes to model the evolution from the zero-age main sequence to the inner BBH merger.

We use COMPAS as described in Appendix A to explore a binary system that is representative of the CHE inner binary for a GW170729-like system. We follow the evolution from the zero-age main sequence until BBH formation. This system initially consists of a circular CHE binary with $M_1 = M_2 = 29\,M_\odot$, $R_1 = R_2 = 4.8\,\mathrm{R}_\odot$, and $a = 10.2\,\mathrm{R}_\odot$. The separation, masses, and radial time evolution are shown in Figure 7. The CHEs are expected to contract throughout their lifetimes (see, e.g., Aguilera-Dena et al. 2018); however, the current implementation of them in COMPAS assumes a fixed radius during the main sequence. The low metallicity results in negligible mass loss, and the orbit barely changes throughout the full evolution. There are two milestones in the evolution. The first one is the evolution after hydrogen depletion (≈6.8 Myr), when each component becomes a $1.8\,\mathrm{R}_\odot$ naked helium star. The final one is the failed supernova (≈7.1 Myr), which reduces the mass by 10% (Appendix A) and increases the separation to $a = 11.6\,\mathrm{R}_\odot$ and

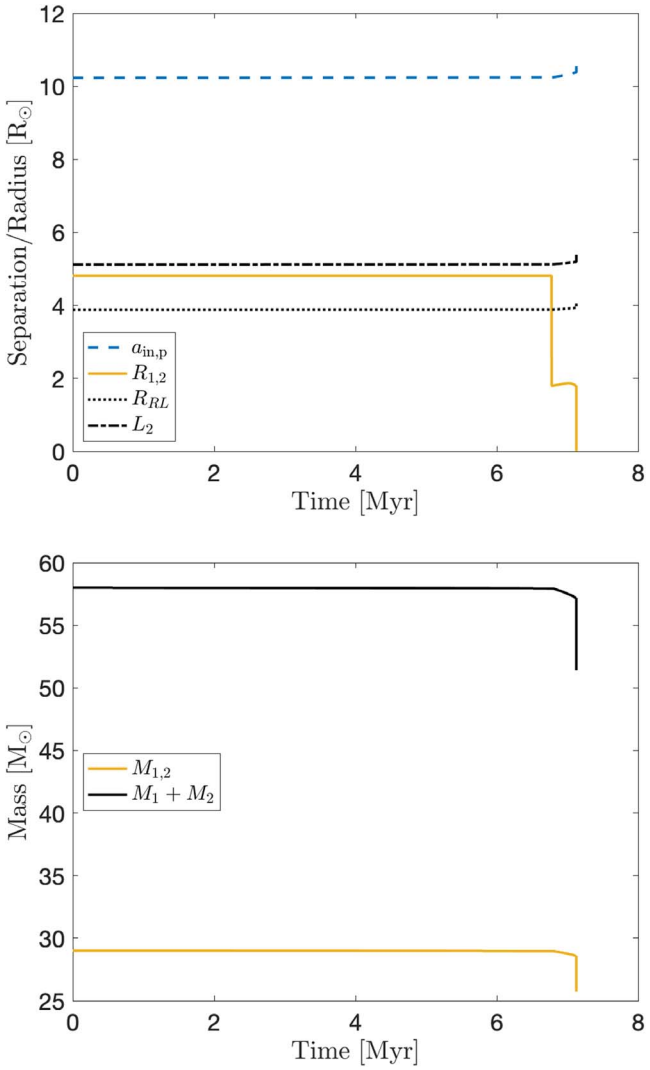


**Figure 7.** COMPAS time evolution, from zero-age main sequence to BBH formation, of a CHE binary at $Z = 10^{-4}$. Top panel: separation (dashed blue), radius (solid yellow), Roche lobe (black dotted), and second Lagrangian point (black dotted–dashed). Bottom panel: individual masses (solid yellow) and total mass (solid black).

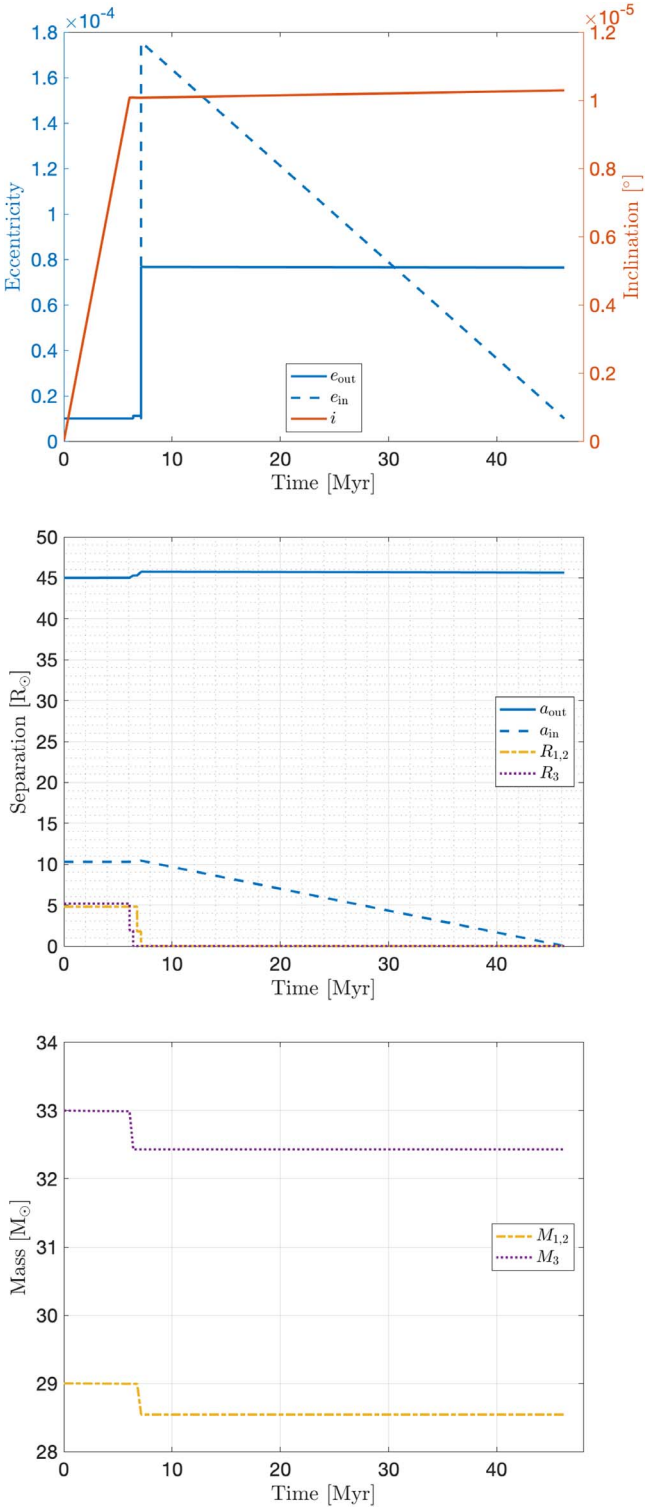


**Figure 8.** The TRES time evolution, from zero-age main sequence to inner BBH merger, of a triple leading to a GW170729-like system (Section 3.4). Top panel: outer eccentricity (solid blue), inner eccentricity (dashed blue), and relative inclination (solid orange). Middle panel: outer separation (solid blue), inner separation (dashed blue), radius of the stars in the inner binary (dotted–dashed yellow), and radius of the tertiary star (dotted purple). Bottom panel: mass of the stars in the inner binary (dotted–dashed yellow) and mass of the tertiary star (dotted purple).

the eccentricity to $e = 0.07$. This BBH merges in ≈76 Myr (Peters 1964).

Additionally, we modified the triple evolution code TRES (Toonen et al. 2016, 2020) to model the evolution from the zero-age main sequence until the BBH coalescence of a compact inner binary of a triple system. The inner binary consists of a CHE system with $M_1 = M_2 = 29\,M_\odot$, $R_1 = R_2 = 4.8\,{\rm R}_\odot$, $a_{\rm in} = 10.3\,{\rm R}_\odot$, and $e_{\rm in} = 10^{-5}$ (this eccentricity is the lower limit allowed in TRES for numerical reasons). Similarly to COMPAS, the radial evolution of all compact stars throughout the main sequence is kept constant. The tertiary is also assumed to be a compact star with $M_3 = 33\,M_\odot$, $R_3 = 5.2\,{\rm R}_\odot$ in an orbit of $a_{\rm out} = 45\,{\rm R}_\odot$, $e_{\rm out} = 10^{-5}$, and relative inclination $i = 0.0$. The complete orbital evolution is shown in Figure 8. There are four milestones in the evolution of this triple system. The first is the formation of an outer $33.4\,M_\odot$ BH at ≈6 Myr. The second is the evolution after hydrogen depletion (≈6.8 Myr), when each component of the inner binary becomes a $1.8\,{\rm R}_\odot$ naked helium star. The third is the supernovae (≈7.1 Myr) of the stars in the inner binary, which result in two BHs of $M_{\rm BH,1} = M_{\rm BH,2} = 28.5\,M_\odot$, $a_{\rm in} = 10.4\,{\rm R}_\odot$, $e_{\rm in} \approx 2 \times 10^{-4}$, $e_{\rm out} \approx 0.8 \times 10^{-4}$, and $i \approx 10^{-5}$. The final milestone is the GW evolution from the inner binary; the inner BBH merges at ≈46 Myr. The triple remains approximately circular and

coplanar throughout the evolution, validating our assumptions at the moment of triple BH formation and throughout the sequential merger.

In summary, we used two independent codes to test the validity of our assumptions in Section 2. With COMPAS, we validate the compact inner binary evolution. We use TRES to do a dynamical calculation to corroborate that, following our initial conditions, there are no major orbital changes that would modify our assumptions during both BBH mergers. Finally, we show that our numerical results are consistent with our semianalytical formalism.

## ORCID iDs

Alejandro Vigna-Gómez https://orcid.org/0000-0003-1817-3586
Silvia Toonen https://orcid.org/0000-0002-2998-7940
Enrico Ramirez-Ruiz https://orcid.org/0000-0003-2558-3102
Nathan W. C. Leigh https://orcid.org/0000-0003-0347-276X
Carl-Johan Haster https://orcid.org/0000-0001-8040-9807

## References

Abbott, B. P., Abbott, R., Abbott, T. D., et al. 2017, CQGra, 34, 044001
Abbott, B. P., Abbott, R., Abbott, T. D., et al. 2019, PhRvX, 9, 031040
Abbott, R., Abbott, T. D., Abraham, S., et al. 2020a, PhRvL, 125, 101102
Abbott, R., Abbott, T. D., Abraham, S., et al. 2020b, ApJ, 900, L13
Abbott, R., Abbott, T. D., Abraham, S., et al. 2020c, ApJL, 896, L44
Abt, H. A. 1983, ARA&A, 21, 343
Aguilera-Dena, D. R., Langer, N., Moriya, T. J., & Schootemeijer, A. 2018, ApJ, 858, 115
Antonini, F., Toonen, S., & Hamers, A. S. 2017, ApJ, 841, 77
Astropy Collaboration, Price-Whelan, A. M., SipHocz, B. M., et al. 2018, AJ, 156, 123
Astropy Collaboration, Robitaille, T. P., Tollerud, E. J., et al. 2013, A&A, 558, A33
Batta, A., & Ramirez-Ruiz, E. 2019, arXiv:1904.04835
Belczynski, K. 2020, arXiv:2009.13526
Belczynski, K., Kalogera, V., & Bulik, T. 2002, ApJ, 572, 407
Blaauw, A. 1961, BAN, 15, 265
Boyle, L., Kesden, M., & Nissanke, S. 2008, PhRvL, 100, 151101
Chatziioannou, K., Cotesta, R., Ghonge, S., et al. 2019, PhRvD, 100, 104015
Costa, G., Bressan, A., Mapelli, M., et al. 2020, arXiv:2010.02242
de Mink, S. E., & Mandel, I. 2016, MNRAS, 460, 3545
de Vries, N., Portegies Zwart, S., & Figueira, J. 2014, MNRAS, 438, 1909
du Buisson, L., Marchant, P., Podsiadlowski, P., et al. 2020, MNRAS, 499, 5941
Farmer, R., Renzo, M., de Mink, S. E., Fishbach, M., & Justham, S. 2020, ApJL, 902, L36
Farmer, R., Renzo, M., de Mink, S. E., Marchant, P., & Justham, S. 2019, ApJ, 887, 53
Farrell, E. J., Groh, J. H., Hirschi, R., et al. 2020, MNRAS, in press (doi:10.1093/mnrasl/slaa196)
Fishbach, M., & Holz, D. E. 2020, ApJL, 904, L26
Fragione, G., & Kocsis, B. 2020, MNRAS, 493, 3920
Fragione, G., Loeb, A., & Rasio, F. A. 2020, ApJL, 895, L15
Fryer, C. L., Belczynski, K., Wiktorowicz, G., et al. 2012, ApJ, 749, 91
Fuller, J., & Ma, L. 2019, ApJL, 881, L1
González, J. A., Sperhake, U., Brügmann, B., Hannam, M., & Husa, S. 2007, PhRvL, 98, 091101
Haster, C.-J., Antonini, F., Kalogera, V., & Mandel, I. 2016a, ApJ, 832, 192
Haster, C.-J., Wang, Z., Berry, C. P. L., et al. 2016b, MNRAS, 457, 4499
He, M. Y., & Petrovich, C. 2018, MNRAS, 474, 20
Heger, A., Fryer, C. L., Woosley, S. E., Langer, N., & Hartmann, D. H. 2003, ApJ, 591, 288
Heger, A., & Woosley, S. E. 2002, ApJ, 567, 532
Hoang, B.-M., Naoz, S., Kocsis, B., Rasio, F. A., & Dosopoulou, F. 2018, ApJ, 856, 140
Hurley, J. R., Pols, O. R., & Tout, C. A. 2000, MNRAS, 315, 543
Iben, I. J., & Tutukov, A. V. 1999, ApJ, 511, 324
Inayoshi, K., Hirai, R., Kinugawa, T., & Hotokezaka, K. 2017, MNRAS, 468, 5020
Jiménez-Forteza, X., Keitel, D., Husa, S., et al. 2017, PhRvD, 95, 064024
Kimball, C., Talbot, C., Berry, C. P. L., et al. 2020, ApJ, 900, 177
Langer, N. 2012, ARA&A, 50, 107
Leigh, N. W. C., & Geller, A. M. 2013, MNRAS, 432, 2474
Leigh, N. W. C., Lützgendorf, N., Geller, A. M., et al. 2014, MNRAS, 444, 29
Leigh, N. W. C., Toonen, S., Portegies Zwart, S. F., & Perna, R. 2020, MNRAS, 496, 1819
LIGO Scientific Collaboration 2018, LIGO Algorithm Library—LALSuite, Free Software (GPL), doi:10.7935/GT1W-FZ16
Lousto, C. O., Campanelli, M., Zlochower, Y., & Nakano, H. 2010, CQGra, 27, 114006
Maeder, A. 1987, A&A, 178, 159
Mangiagli, A., Bonetti, M., Sesana, A., & Colpi, M. 2019, ApJL, 883, L27
Marchant, P., Langer, N., Podsiadlowski, P., Tauris, T. M., & Moriya, T. J. 2016, A&A, 588, A50
Mardling, R. A., & Aarseth, S. J. 2001, MNRAS, 321, 398
Marigo, P., Girardi, L., Chiosi, C., & Wood, P. R. 2001, A&A, 371, 152
Martinez, M. A. S., Fragione, G., Kremer, K., et al. 2020, ApJ, 903, 67
Miller, M. C., & Colbert, E. J. M. 2004, IJMPD, 13, 1
Moe, M., & Di Stefano, R. 2017, ApJS, 230, 15
Müller, B., Heger, A., Liptai, D., & Cameron, J. B. 2016, MNRAS, 460, 742
Naoz, S. 2016, ARA&A, 54, 441
Neijssel, C. J., Vigna-Gómez, A., Stevenson, S., et al. 2019, MNRAS, 490, 3740
Öpik, E. 1924, PTarO, 25, 6
Peters, P. C. 1964, PhRv, 136, B1224
Planck Collaboration, Ade, P. A. R., Aghanim, N., et al. 2016, A&A, 594, A13
Podsiadlowski, P., Joss, P. C., & Hsu, J. J. L. 1992, ApJ, 391, 246
Portegies Zwart, S. F., & McMillan, S. L. W. 2000, ApJL, 528, L17
Riley, J., Mandel, I., Marchant, P., et al. 2020, arXiv:2010.00002
Rodriguez, C. L., Zevin, M., Amaro-Seoane, P., et al. 2019, PhRvD, 100, 043027
Safarzadeh, M., Hamers, A. S., Loeb, A., & Berger, E. 2020, ApJL, 888, L3
Samsing, J., & Hotokezaka, K. 2020, arXiv:2006.09744
Sana, H., de Mink, S. E., de Koter, A., et al. 2012, Sci, 337, 444
Sana, H., Le Bouquin, J.-B., Lacour, S., et al. 2014, ApJS, 215, 15
Shenar, T., Gilkis, A., Vink, J. S., Sana, H., & Sander, A. A. C. 2020, A&A, 634, A79
Sigurdsson, S., & Hernquist, L. 1993, Natur, 364, 423
Stevenson, S., Sampson, M., Powell, J., et al. 2019, ApJ, 882, 121
Stevenson, S., Vigna-Gómez, A., Mandel, I., et al. 2017, NatCo, 8, 14906
Tanikawa, A., Kinugawa, T., Yoshida, T., Hijikawa, K., & Umeda, H. 2020, arXiv:2010.07616
Tokovinin, A. 2017, ApJ, 844, 103
Toonen, S., Hamers, A., & Portegies Zwart, S. 2016, ComAC, 3, 6
Toonen, S., Portegies Zwart, S., Hamers, A. S., & Bandopadhyay, D. 2020, A&A, 640, A16
van Son, L. A. C., De Mink, S. E., Broekgaarden, F. S., et al. 2020, ApJ, 897, 100
Vigna-Gómez, A., Justham, S., Mandel, I., de Mink, S. E., & Podsiadlowski, P. 2019, ApJL, 876, L29
Vigna-Gómez, A., Neijssel, C. J., Stevenson, S., et al. 2018, MNRAS, 481, 4009